Systematic feasibility analysis of performing elastography using reduced dose CT lung image pairs

Katelyn Hasse[a)]
Department of Radiation Oncology, University of California, Los Angeles, Los Angeles, CA 90095, USA

Scott S. Hsieh
Department of Radiology, University of California, Los Angeles, Los Angeles, CA 90095, USA

Dylan O'Connell, Bradley Stiehl, Yugang Min, John Neylon, Daniel A. Low, and Anand P. Santhanam
Department of Radiation Oncology, University of California, Los Angeles, Los Angeles, CA 90095, USA

(Received 22 July 2019; revised 20 February 2020; accepted for publication 23 February 2020; published xx xxxx xxxx)

Purpose: Elastography using computer tomography (CT) is a promising methodology that can provide patient-specific regional distributions of lung biomechanical properties. The purpose of this paper is to investigate the feasibility of performing elastography using simulated lower dose CT scans.
Methods: A cohort of eight patient CT image pairs were acquired with a tube current–time product of 40 mAs for estimating baseline lung elastography results. Synthetic low mAs CT scans were generated from the baseline scans to simulate the additional noise that would be present in acquisitions at 30, 25, and 20 mAs, respectively. For the simulated low mAs scans, exhalation and inhalation datasets were registered using an in-house optical flow deformable image registration algorithm. The registered deformation vector fields (DVFs) were taken to be ground truth for the elastography process. A model-based elasticity estimation was performed for each of the reduced mAs datasets, in which the goal was to optimize the elasticity distribution that best represented their respective DVFs. The estimated elasticity and the DVF distributions of the reduced mAs scans were then compared with the baseline elasticity results for quantitative accuracy purposes.
Results: The DVFs for the low mAs and baseline scans differed from each other by an average of 1.41 mm, which can be attributed to the noise added by the simulated reduction in mAs. However, the elastography results using the DVFs from the reduced mAs scans were similar from the baseline results, with an average elasticity difference of 0.65, 0.71, and 0.76 kPa, respectively. This illustrates that elastography can provide equivalent results using low-dose CT scans.
Conclusions: Elastography can be performed equivalently using CT image pairs acquired with as low as 20 mAs. This expands the potential applications of CT-based elastography. © *2020 American Association of Physicists in Medicine* [https://doi.org/10.1002/mp.14112]

Key words: low-dose CT, lung elastography, simulated noise

1. INTRODUCTION

Chronic obstructive pulmonary disease (COPD) is a major cause of disability and the third leading cause of death in the United States.[1] COPD refers to a large group of incurable lung diseases characterized by the persistent reduction of lung function. Changes in lung function are associated with changes in lung tissue biomechanical properties; for example, diseases of the lung that alter lung function often do so by altering the amounts of elastin and collagen of parenchymal tissue, leading to changes in tissue elasticity.[2] Excised tissue studies have shown that localized changes in the biomechanical properties of lung parenchyma precede the initiation and progression of certain lung diseases, including cancer.[3,4] While computed tomography (CT) is commonly used for lung imaging, it does not present an explicitly quantitative characterization of the lung biomechanical properties.[5]

Elastography has the potential to inform diffuse lung disease phenotype characterization and staging and treatment response monitoring. Elastography is a noninvasive method of mapping the distribution of a critical lung biomechanical property, elasticity, or tissue stiffness, generally performed with ultrasound techniques.[6] The elasticity of tissue can be used to differentiate regions of diseased tissue (such as COPD or cancer) from functional tissue. In our preliminary work, we demonstrated a novel elastography approach more applicable to radiation therapy using simulated virtual lung phantoms.[7] This methodology was quantified and validated for lung cancer radiation therapy CT scans reconstructed using a published breathing motion model.[8]

Our elastography estimation method used multiple fast helical CT scans, each delivering 1.2 mSv to the lungs. The original protocol utilized 25, 40 mAs scans, but Thomas et al and O'Connell, et al determined that minima of 10 and 6 scans would be required for ungated and prospectively gated

protocols, corresponding to a total effective dose of 12 and 7.2 mSv, respectively.[9,10] Mettler, et al showed that the published dose range for routine diagnostic CT scans ranges from 4.0 to 18.9 mSv, with an average of 7 mSv.[11] Currently, SPIROMICS studies have employed an effective imaging dose as low as 4.9 mSv in their protocols for acquiring image pairs.[12] Low-dose CT studies using iterative reconstruction have reported effective doses below 1 mSv. Our current technique delivers exposures similar to routine diagnostic CT studies. Diagnostic CT studies are used for human image interpretation while the scans acquired for elastography estimation are used to quantitatively determine the motion and distortion characteristics of lung tissues during breathing. While the estimation method is agnostic to the underlying CT dose, variations in the CT dose is considered as the primary reason for a lowered accuracy in the estimated elasticity. Therefore, the aim of this paper is to assess the effect of image noise on elastography quality using simulated reduced dose CT scans.

2. MATERIALS AND METHODS

This study used a cohort of CT datasets of eight radiotherapy patients that were acquired under IRB # 11-000620-CR-00004 at UCLA.[13] The patients underwent a series of 25 fast low-dose helical CT scans. The scans were co-registered using DEEDs. The resulting deformation vector fields (DVFs), along with the breathing amplitude and rate, were used to develop patient-specific breathing motion models [termed five-dimensional CT (5DCT) models].[13] Exhalation and inhalation, defined as the 5th and 85th percentile tidal volume, were reconstructed using the 5DCT model. Unlike the published 5DCT approach, where multiple deformed scans are averaged to reduce noise, only a single CT scan was deformed to represent these tidal volumes to maintain the noise characteristics of the original fast helical (1.2 mSv) scans, termed the baseline scans. The CT parameters are listed in Table I.

2.A. Low-dose CT simulation

Noise was injected in the image domain of the baseline scans to simulate the effects of lower dose scanning. As lowering the tube current is the most direct way of achieving radiation dose reduction, different tube currents were simulated as a way of replicating the additional noise of lower dose scans.[14] The noise injection process used forward projection to estimate raw data,[15] calculated appropriate photon statistics, and finally back projected added and filtered noise.

TABLE I. Relevant computed tomography (CT) scan parameters.

Single collimation width	0.6 mm
Total collimation width	19.2 mm
Spiral Pitch Factor	1.5
Table Speed	87.2 mm/s
CTDIvol	3.04 mGy
kVp	120
Effective mAs	40
Tube rotation time	330 ms
X-ray tube current	182 mA

2.A.1. Noise injection process

Noise was injected on each slice independently, neglecting the cone angle of the system and assuming it was similar to a fan-beam geometry. Each slice was forward projected to estimate the attenuation of each ray, and we included the effect of a bowtie filter following the attenuation profile described in Ref. [21] which was for a different system. We assumed that the scanner used a rebin-to-parallel reconstruction scheme to preserve noise uniformity and hence sampled rays in a parallel beam fashion.

The number of photons incident on the detector was calculated by estimating that 1.8×106 photons/mm^2-mAs arrived at the detector in the absence of attenuation for a typical spectrum at 120 kVp.[22] The number of photons was then multiplied by an efficiency factor E that incorporated effects such as geometric efficiency, and noise from scatter or Swank factor was added. E was selected by comparison to experimental measurements, explained below. This noise-addition sinogram was then filtered by a smoothing function $s(x)$ to match the noise power spectrum (NPS). The noise-addition sinogram was then reconstructed and added to the original image to synthesize the reduced dose CT scan. The scans were acquired without tube current modulation. In order to provide a conservative estimate of possible dose reduction, we assumed that the original scans were noiseless.

The efficiency factor E and smoothing function $s(x)$ were tuned to reconstructions of a water cylinder scanned using the same protocol as the clinical series. The water phantom was a component of the ACR phantom, scanned with a Siemens Definition AS. The scan was performed at 120 kVp and 500 mA with a rotation time of 0.5 s, a collimation of 19.2 mm at isocenter, and a pitch value of 1. The reconstruction was performed using a B30 kernel and 1 mm slice thickness. The water cylinder image was binarized (thresholded to either −1000 or 0 HU) to create a simulated noiseless water cylinder, and noise was injected into the binarized water cylinder to simulate the noise in the experimental measurements. The one-dimensional (1D) NPS was calculated for comparison. The calculation of the NPS has been described in greater detail elsewhere[23,24] but briefly, seven adjacent slices were averaged to alleviate through-plane correlations, a series of square region of interests (ROIs) with side length 31 mm and each positioned 30 mm from the center of the water cylinder were defined, and their Fourier transforms were taken after mean subtraction to create the NPS. These NPS measurements were averaged and binned in the radial direction to produce 1D NPS. To match the simulated NPS with experimental NPS, we selected an efficiency factor of

E = 59% and a Gaussian smoothing filter with standard deviation of 0.43 channels.

Figure 1 shows the experimental against simulated noise in a water cylinder, and Fig. 2 shows the estimated noise power spectra. Agreement of the noise power spectra is moderate at low frequencies, presumably due to low frequency artifacts which may arise from imperfect correction of scatter or beam hardening. The spatial distributions of the noise as seen in Fig. 1 differed slightly from each other, possibly because we employed a generic bowtie filter profile.

For each patient dataset, noise was injected to represent CT scans acquired with reduced tube current–time products of 30, 25, and 20 mAs. The lower limit of 20 mAs was selected to match the lower end of lung cancer screening and emphysema detection programs.[14]

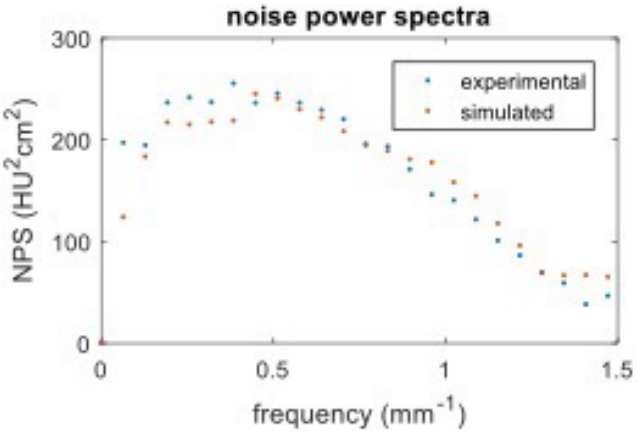

FIG. 2. Comparison of noisy power spectra from simulated and experimental data.

2.B. Image registration

The model-guided elasticity approach presented in this study relies on DVFs extracted from deformable image registration (DIR) of exhalation and inhalation breathing phases. The lungs were segmented using an intensity thresholding approach, and the two breathing phases were deformably registered using a well-validated in-house multilevel optical flow DIR algorithm.[16] The DVFs of the baseline images were taken to be the ground truth displacement for the elasticity estimation process.

2.C. Elasticity estimation

The elasticity estimation process has been systematically studied and validated for the lungs in Ref. [7,8]; for clarity, the process will be summarized briefly here. The inverse elasticity problem was formulated as a parameter-optimization problem with an objective to determine the elasticity parameter that would minimize the difference between ground truth (registration) DVFs and those computed by a constitutive biomechanical model.[17] Solving the inverse elasticity problem was conducted in two steps: (a) estimating the DVF for every voxel of lung tissue for a given elasticity distribution and boundary constraint using a biomechanical model; and (b) optimizing the elasticity distribution to best reproduce the registration ground truth DVF.

The elasticity results derived for the baseline CT scans will be considered ground truth and used for comparison to the lower mAs results.

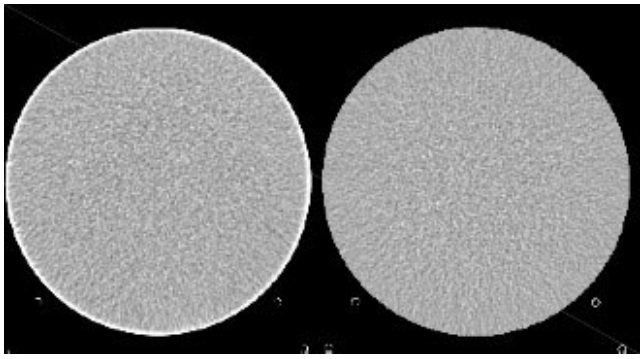

FIG. 1. (Left) Experimental reconstruction of water cylinder.[25] (Right) Simulated injection of noise. Average of 7 slices. WW = 100 HU.

2.D. Quantitative analysis

As a first measure of quantitative analysis, the displacement results from each of the lower mAs model-guided elasticity estimations were evaluated and compared with those obtained with the baseline CT scans. The comparison was first performed using average and maximum values. Absolute error between the distributions was then calculated by subtracting the lower mAs DVFs from the baseline DVFs. We then computed the number of voxels whose estimated DVF errors were <0.5 or 1 mm. Equivalent analyses were conducted for the elasticity estimates, with an error threshold of 0.5 or 3 kPa.

For further investigation of the elasticity distribution, the underlying elasticity values were split into low elasticity, representing voxels with elasticity values between 1 and 3 kPa, mid elasticity, representing voxels with elasticity values between 3 and 6 kPa, and high elasticity, representing voxels with elasticity values >6 kPa, subgroups. The error within each of the elasticity ranges is relevant since parenchymal tissue, specifically diseased parenchymal tissue, is known to have low elasticity values.

In addition to the previous evaluation, the normalized cross-correlation (NCC) image similarity metric was used to further assess the results of our study. NCC is a similarity measure that is invariant to brightness and contrast variations that has been previously used to compare similarity of medical lung image.[18] NCC is relatively insensitive to intensity changes caused by tissue compression difference between different breathing phases.[19] NCC values range from a perfect match of 1 to a completely anti-correlated match of −1, and were calculated for every 2D slice. These values were then averaged over the whole 3D image volume for comparison.

3. RESULTS

3.A. Low-dose CT simulation

Figure 3 shows an example of a baseline exhalation lung scan (a), a simulated 30 mAs lung scan (b), and a simulated 20 mAs lung scan. The reduced dose images are noisier than the baseline image, as expected, especially in the soft tissue regions of the scan. This illustrates the effect of the addition of the noise on 2D slices of the 3D volumes that were investigated. Table II quantitates the perceived noisiness. The values in Table II represent the standard deviation of HU values taken from an ROI in the liver of each patient, averaged over all of the patients. It can be seen that the noise increases with the decrease of mAs.

3.B. Image registration

An example of the registration results for both a baseline and 20 mAs scan pair is shown in Fig. 4. Although the registration was performed in 3D, 2D slices have been shown for clarity. Figures. 4(a) and 4(c) show the exhalation superimposed with inhalation. Mismatches can be seen between the exhalation and inhalation images, especially near the base of the lung. Figures. 4(b) and 4(d) show the overlay between the warped exhalation and inhalation images. The registration accounts for the lung deformation well, with little mismatch seen between the warped end-exhalation and end-inhalation images, for both the baseline and reduced mAs scans. The registration accuracy visually appears to be similar, regardless of injected noise.

3.C. Quantitative analysis

Table III shows the maximum and average voxel displacements for the baseline, and simulated reduced mAs scans for all patients. The first column indicated the maximum value over all patients, while the subsequent columns indicate the displacement errors averaged over all of the considered patients. For each dataset, the model-generated displacement vectors were compared with the registration-generated effective ground truth displacement vectors, and the average displacement error and percent of voxels with error <1 and 0.5 mm were tabulated. A two-sample t test considering a significance level of 0.05 showed that all of the tabulated values for the simulated 20 mAs scans were not significantly different than the baseline displacement values.

TABLE II. Quantitative example of noise values calculated by taking the standard deviation of an ROI in the liver of each patient.

Average	Std. Dev. Of ROI in soft tissue (HU)
Baseline (40 mAs)	42.88
30 mAs	104.40
25 mAs	123.58
20 mAs	153.16

It can be seen that the displacement metrics obtained for all three mAs levels were quite similar to the baseline scans. The error increased most at 20 mAs, but were reasonable with respect to the baseline results. This supports the fact that the displacement results for the elastography process remain similar to the baseline even with the mAs reduced to 20.

Figure 5(a) shows the estimated elasticity distributions for a 2D slice of a baseline CT scan. Figure 5(b)–5(d) shows the absolute difference between the baseline scan and 30 mAs (b), 25 mAs (c), and 20 mAs (d) scans. On average, the error was <0.62 kPa, which is small compared to the average lung elasticity of 6.59 kPa. The highest error was seen near the lower lobes of the lung, where displacement would be greatest. This is further illustrated in Table IV. Table IV quantitates the elasticity error between that estimated from the baseline and reduced mAs scans. Maximum elasticity error (over all patients), average elasticity error, and error <0.5 and 3 kPa (averaged over all of the considered patients) are listed for each dose reduction. The individual column values were averaged over all of the considered patients. The elasticity error increases as the dose is reduced; however, even with a current–time product of 20 mAs, the average elasticity error remained <0.76 kPa.

Table V shows the percentages of voxels in which the low-dose elasticity estimations converged within 1 kPa of the baseline elasticity estimation results, binned by underlying elasticity value. It can be seen that the high-elasticity bin had the most error. Since lung diseases, such as diffuse lung disease and COPD, are known to be associated with lower than normal values, this result supports the fact that low-dose CT elastography can be performed accurately for these patients.

Table VI shows the NCC values between (a) the reduced mAs and baseline ground truth displacement, (b) the reduced mAs and baseline-estimated elasticity distributions, and (c) the reduced mAs ground truth and model displacement. The reduced mAs displacement values were similar to the

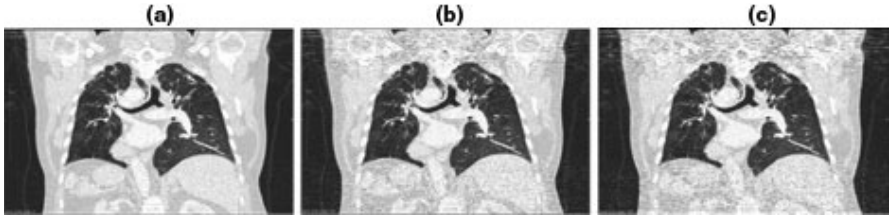

FIG. 3. Example of exhalation lung baseline (a), 30 mAs (b), and 20 mAs (c) scans.

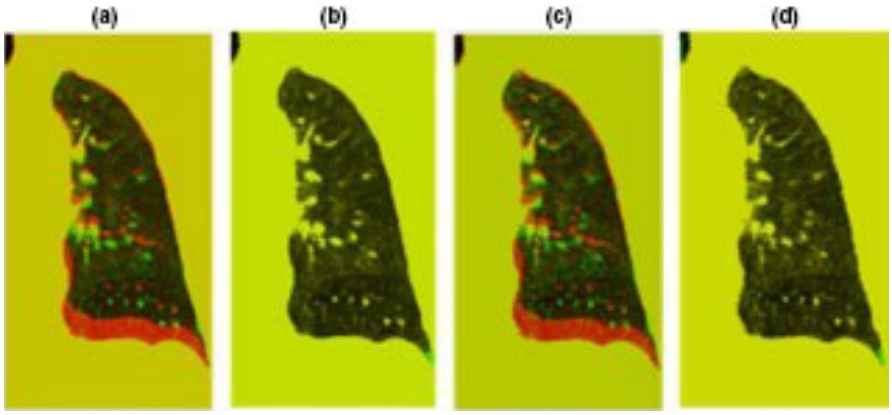

FIG. 4. Example of registration for baseline (a & b) and 20 mAs (c & d) CT scans. (a & c) show the endexhalation overlain with end-inhalation. (b & d) show the warped exhalation superimposed with inhalation.

TABLE III. Maximum displacement results over all patients and average displacement error results for original, and reduced mAs scans.

Average	Maximum displacement (mm)	Average displacement (mm)	Average displacement error (mm)	Error < 1 mm (%)	Error < 0.5 mm (%)
Baseline (40 mAs)	13.79	4.89	0.42 ± 0.31	84.02	65.08
30 mAs	12.01	4.08	0.52 ± 1.52	85.03	65.27
25 mAs	13.72	4.27	0.53 ± 1.53	84.96	63.91
20 mAs	12.46	4.21	0.56 ± 1.56	84.00	62.08

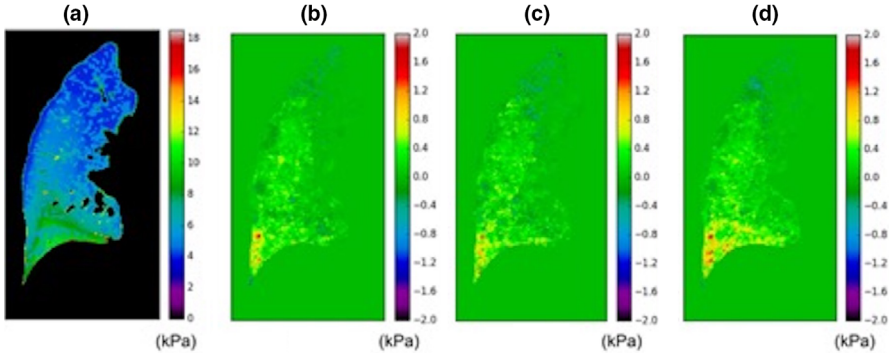

FIG. 5. Estimated elasticity distribution in kPa for baseline CT scan (a). Absolute difference between baseline and 30 mAs (b), 25 mAs (c), and 20 mAs (d) scans.

TABLE IV. Maximum elasticity error results and average elasticity error results between the baseline-estimated elasticity and reduced mAs-estimated elasticity.

	Maximum elasticity error (kPa)	Average elasticity error (kPa)	Error < 0.5 kPa (%)	Error < 3 kPa (%)
30 mAs	7.25	0.65	75.56	92.44
25 mAs	6.96	0.71	71.46	92.27
20 mAs	7.40	0.76	68.07	91.70

TABLE V. Elasticity errors for low, mid, and high-elasticity bins for each low mAs simulation.

	Low elasticity range error < 1 kPa (%)	Mid elasticity range error < 1 kPa (%)	High-elasticity range error < 1 kPa (%)
Average	95.81	94.13	63.81
30 mAs	96.85	94.95	66.86
25 mAs	95.67	94.11	63.99
20 mAs	94.91	93.32	60.59

baseline displacement values, with similarity decreasing with decreased mAs as expected. However, the estimated elasticity distributions were similar in all cases, as were the effective ground truth and model displacements for each mAs reduction. This demonstrates that low-dose CT-based model displacements can be used to characterize lung tissue deformations during breathing.

The NCC values for 30, 25, and 20 mAs are very similar, illustrating that current–time product could be reduced to as low as 20 mAs and still provide equivalent elastography results. A two-sample t test considering a significance level of 0.05 was performed and did not show significant difference, though claims of significance are precluded by the small sample size.

4. DISCUSSION

In this study, low mAs CT scans were simulated using a noise injection process in order to determine the effect of noise on our lung elastography process. Simulated scans with tube current–time products representing 30, 25, and 20 mAs were investigated. The results of the baseline scans and low mAs simulated scans were similar indicating that low-dose CT scans could produce reliable elastography results. For example, 20 mAs scans had greater than 94% accuracy when used for elastography purposes when compared to baseline. Since the baseline scans were taken with mAs of 40 mAs and an effective dose of 1.2 mSv, this suggests that the effective dose could be reduced to about 0.6 mSv per scan while still obtaining useful elastographic information. In order to find the lower dose limit for elastography assessment, scans with simulated tube current–time products below 20 mAs will be investigated in future studies.

We identify a few limitations to this study. Firstly, the noise injection code assumed no tube current modulation, which is not typically employed in radiation therapy but is often employed for diagnostic purposes. The algorithms to select tube current modulation are proprietary and depend on the capability of the x-ray generator, which place limits on the slew rate of the tube current. The lack of modulation creates increased noise at the top or bottom of the image as the shoulders or abdomen starts to appear. However, as the parenchymal tissue is located near the center of the image on the chest CT, we believe these artifacts will not affect the parenchymal registration process.

Secondly, the quality of the elastography results depends on the quality of the DIR, which is affected by the addition of noise. The displacement-based error evaluation was performed in order to attempt to quantify the effects of the additional noise. DVFs are highly dependent on pre-processing steps; however, the DVFs were obtained in the same manner for both baseline and low mAs results to ensure a fair elastography comparison. In the future, registration algorithms that are more robust to high imaging noise will be investigated. Furthermore, as the intent of this study was to assess the impact of noise, no noise mitigation techniques were employed, which can be investigated before clinical application.

Thirdly, we employed image domain-based noise injection performed using simulation of the filtered backprojection process. This captures some of the spectral characteristics and noise statistics of the data, but it is not as accurate as noise injection in the raw data domain[20] or actual collection of data at reduced dose. In particular, our process of noise injection through simulated noise filtered backprojection does not capture through-plane noise correlations, may not accurately model tube current modulation, and does not perfectly capture the spectral characteristics of the reconstructed data at high frequencies as our apodization filter was empirically tuned rather than perfectly matched with the reconstruction kernel used to generate the original image data. An alternative approach is to add in colored noise to the image domain directly, shaping the noise spectrum to match typical regions within the patient. This option makes comparatively fewer assumptions and is attractive because of its simplicity. However, it does assume that the noise is stationary, which is violated in highly attenuating regions where noise streaks occur. In general, noise injection into images is not a standard technique because it is generally accepted that all existing solutions require approximations. Future work will focus on extending the noise injection technique to the raw data domain, which requires prospective collection of raw data but has much improved accuracy.

Finally, the sample size for this analysis was small and precluded any claims of statistical significance. More data will be collected and analyzed in the future to ensure the results are statistically significant.

5. CONCLUSIONS

Our study suggests that pairs of CT scans acquired with as low as 20 mAs each could be used to reliably perform elastography, exposing the patient to a total dose of 1.2 mSv, substantially less than the average diagnostic CT effective dose. These results indicated the feasibility of performing elastography using low mAs CT scans, expanding the potential of CT-based elastography.

TABLE VI. Image similarity metrics between the baseline and reduced mAs ground truth displacement, reduced mAs ground truth and model displacement, and baseline and reduced mAs elasticity.

NCC (mAs)	Low-dose displacement vs baseline displacement	Low mAs estimated elasticity vs baseline estimated elasticity	Low mAs ground truth displacement vs low mAs model displacement
30	0.987	0.977	0.986
25	0.984	0.975	0.986
20s	0.984	0.973	0.985

ACKNOWLEDGMENT

This material is based on the work supported by the National Science Foundation Graduate Research Fellowship under Grant No. DGE-1144087 and the Ken and Wendy Ruby Foundation.

CONFLICT OF INTEREST

The authors declares there is no conflict of interest in this article

[a)]Author to whom correspondence should be addressed. Electronic mail: khasse@ucla.edu.

REFERENCES

1. National Center for Chronic Disease Prevention and Health Promotion. D.o.P.H. Chronic Obstructive Pulmonary Disease (COPD); 2017. Available from: https://www.cdc.gov/copd/index.html.
2. Risholm P, Ross J, Washko GR, Wells WM. Probabilistic elastography: estimating lung elasticity. *Inf Process Med Imaging*. 2011;6801:699–710.
3. Suki B, Stamenovic D, Hubmayr R. Lung parenchymal mechanics. *Compr Physiol*. 2011;1:1317–1351.
4. Suki B, Bates JH. Extracellular matrix mechanics in lung parenchymal diseases. *Respir Physiol Neurobiol*. 2008;163:33–43.
5. Fredman AJ, Frolik JL, Garra BS. Lung strain profiles using computed tomography elastography. *Conf Proc IEEE Eng Med Biol Soc*. 2004;2:1545–1548.
6. Ophir J, Alam SK, Garra BS, et al. Elastography: imaging the elastic properties of soft tissues with ultrasound. *J Med Ultrason*. 2001;2002:155.
7. Hasse K, Neylon J, Santhanam AP. Feasibility and quantitative analysis of a biomechanical model-guided lung elastography for radiotherapy. *Biomed Phys Eng Express*. 2017;3:025006.
8. Hasse K, O'Connell D, Min Y, et al. Estimation and validation of patient-specific high-resolution lung elasticity derived from 4DCT. *Med Phys*. 2017;45:666–677.
9. Thomas DH, Ruan D, Williams P, et al. Is there an ideal set of prospective scan acquisition phases for fast-helical based 4D-CT? *Phys Med Biol*. 2016;61:N632–N641.
10. O'Connell D, Ruan D, Thomas DH, et al. A prospective gating method to acquire a diverse set of free-breathing CT images for model-based 4DCT. *Phys Med Biol*. 2018;63:04NT03.
11. Mettler FA Jr, Huda W, Yoshizumi TT, Mahesh M. Effective doses in radiology and diagnostic nuclear medicine: a catalog. *Radiology*. 2008;248:254–263.
12. Yin Y, Raffy P, Sieren JP, et al. Quantitative CT in spiromics: lobar evaluation via image warping of Tlc masks Onto Rv images. *Am J Respir Crit Care Med*. 2014;189.
13. Low DA, White BM, Lee PP, et al. A novel CT acquisition and analysis technique for breathing motion modeling. *Phys Med Biol*. 2013;58:L31–L36.
14. Kubo T, Lin PJ, Stiller W, et al. Radiation dose reduction in chest CT: a review. *AJR Am J Roentgenol*. 2008;190:335–343.
15. Li X, Samei E, DeLong DM, et al. Pediatric MDCT: towards assessing the diagnostic influence of dose reduction on the detection of small lung nodules. *Acad Radiol*. 2009;16:872–880.
16. Min YG, Neylon J, Shah A, et al. 4D-CT Lung registration using anatomy-based multi-level multi-resolution optical flow analysis and thin-plate splines. *Int Jour Comp Ass Radiol Surg*. 2014;9:875–889.
17. Neylon J, Qi X, Sheng K, et al. A GPU based high-resolution multilevel biomechanical head and neck model for validating deformable image registration. *Med Phys*. 2015;42:232–243.
18. Zhao F, Huang QM, Gao W. Image matching by normalized cross-correlation. 2006 IEEE International Conference on Acoustics, Speech and Signal Processing, Vols 1–13; 2006: 1977–1980.
19. Avants BB, Epstein CL, Grossman M, Gee JC. Symmetric diffeomorphic image registration with cross-correlation: evaluating automated labeling of elderly and neurodegenerative brain. *Med Image Analys*. 2008;12:26–41.
20. Mayo JR, Whittall KP, Leung AN, et al. Simulated dose reduction in conventional chest CT: validation study. *Radiology*. 1997;202:453–457.
21. McKenney SE, Nosratieh A, Gelskey D, et al. Experimental validation of a method characterizing bow tie filters in CT scanners using a real-time dose probe. *Med Phys*. 2011;38:1406–1415.
22. Punnoose J, Xu J, Sisniega A, et al. Technical note: spektr 3.0-A computational tool for x-ray spectrum modeling and analysis. *Med Phys*. 2016;43:4711.
23. Boedeker KL, Cooper VN, McNitt-Gray MF. Application of the noise power spectrum in modern diagnostic MDCT: part I. Measurement of noise power spectra and noise equivalent quanta. *Phys Med Biol*. 2007;52:4027–4046.
24. Friedman SN, Fung GS, Siewerdsen JH, Tsui BM. A simple approach to measure computed tomography (CT) modulation transfer function (MTF) and noise-power spectrum (NPS) using the American College of Radiology (ACR) accreditation phantom. *Med Phys*. 2013;40:051907.
25. Barker BL, Brightling CE. Phenotyping the heterogeneity of chronic obstructive pulmonary disease. *Clin Sci (Lond)*. 2013;124:371–387.